Effects of Rubber Content and Temperature on Dynamic Fracture Toughness of ABS Materials

YANCHUN HAN, RALF LACH, WOLFGANG GRELLMANN

Department of Materials Science, Martin-Luther-University Halle-Wittenberg, D-06099 Halle (Saale), Germany

Received 11 March 1999; accepted 21 July 1999

ABSTRACT: The effects of rubber content and temperature on dynamic fracture toughness of ABS materials have been investigated based on the *J*-integral and crack opening displacement (COD, δ) concepts by an instrumented Charpy impact test. A multiple specimens R-curve method and stop block technique are used. It is shown that the materials exhibit a different toughness behavior, depending on rubber content and temperature. The resistance against stable crack initiation ($J_{0.2}$ or $\delta_{0.2}$) increases with increasing rubber content. However, $J_{0.2}$ first increased with increasing temperature until reaching the maximum value; after that, it decreases with further increasing the temperature. © 2000 John Wiley & Sons, Inc. J Appl Polym Sci 75: 1605–1614, 2000

Key words: ABS materials; instrumented Charpy impact test; *J*-integral; crack opening displacement (COD)

INTRODUCTION

Polymers have been used increasingly as structural materials in industrial applications. It is very important to be able to assure safety against fracture. In this respect, fracture toughness property of polymers plays a crucial role in material design and selection. Noncrystalline polymers such as polystyrene (PS) and poly (methyl methacrylate) (PMMA) exhibit brittle behavior at room temperature, particularly under conditions of sharp notch, plane strain, and high rates of deformation. Great efforts have been made towards developing effective toughening methods for amorphous polymers. Substantial enhancement of the toughness of brittle polymers can be achieved by dispersing elastomeric inclusions or rubber particles in the polymer matrix. However, there is an inevitable reduction in stiffness and tensile strength of polymers by the addition of the rubber phase. But these deficiencies are far outweighed by the gains in fracture resistance. The dispersed rubbery particles act as stress concentrators, favoring the dissipation of the impact energy. An optimum particle size, a low interfacial energy, and good adhesion to the matrix are the necessary requirements for efficient toughening.[1] The major toughening mechanisms are mostly rubber induced multiple crazing and shear yielding of the matrix.

Dynamic fracture testing is of great interest, because many structural components are subjected to high loading rates in normal service, or must survive dynamic loading during accident or unscheduled conditions. Thus, these components must be design against crack initiation under high loading rates. Therefore, design calculations require reliable dynamic fracture toughness data. The dynamic fracture toughness measured at the high loading rates gives more realistic basis for design and integrity evaluation of dynamically loaded structural components. The Charpy impact test has been one of the most popular dy-

Correspondence to: Y. Han, at Changchun Institute of Applied Chemistry, Chinese Academy of Sciences, Changchun 130022, P. R. China

Contract grant sponsor: DFG.

Journal of Applied Polymer Science, Vol. 75, 1605–1614 (2000)

namic fracture tests. The instrumented Charpy impact tester avoids the drawbacks of normal designs and makes the impact testing more reliable and appropriate from the fracture mechanics point of view.

Linear elastic fracture mechanics (LEFM), originally developed to characterize metals, has been used to evaluate the fracture behavior of many brittle polymers. The plane strain fracture toughness parameter, such as the critical stress intensity factor, K_c, or the critical strain energy release rate, G_c, is sufficient to characterize this fracture at its critical condition. The LEFM method is not suitable for rubber-toughened polymers because considerable input energy to the material is dissipated, creating plastic deformation ahead of crack tip. The J-integral concept, introduced by Rice[2] or Begley and Landes,[3] has been successful in describing the fracture in many ductile polymers.[4–8] The J-integral is an energy-based parameter used to characterize the stress and strain fields near a crack tip surrounded by a small scale plasticity. It can be used as a criterion for crack initiation in the fracture of elastic-plastic materials. Thus, the critical J-integral value, J_c, represents the energy required to initiate crack growth. The procedure for determination J_c has been outlined in ASTM E813. Three versions of the ASTM E813 standard are available, i.e., E813-81, E813-87, and E813-89.[9–11] In the ASTM E813-81, the crack growth process is fitted to a straight line. The interaction of the linear regression line with a theoretically predicted blunting line is defined as J_c. However, the crack growth process is fitted to a power law in ASTM E813-87. And the intersection of the power law regression line with the 0.2 mm offset of the blunting line represents J_c. It has been reported by Lee et al.[12,13] that J_c values obtained from the E813-87 are considerably higher that those obtained from the E813-81 method.

In this work, the rubber content and temperature effects on the dynamic fracture toughness of ABS materials have been investigated by means of the J-integral method.

EXPERIMENTAL

Materials and Samples

The materials used in this study are ABS materials with particle diameter of 330 nm and rubber content of 16, 20, 24, 28, and 36%, respectively.

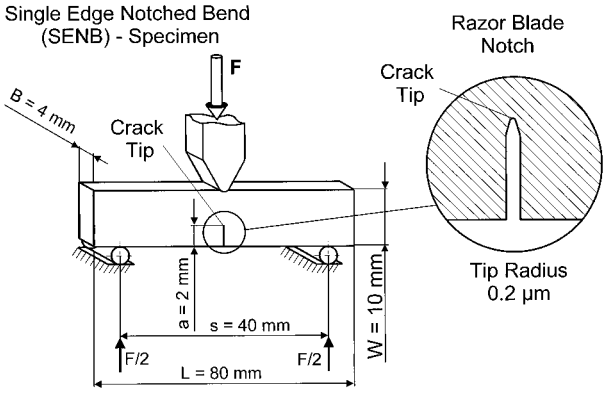

Figure 1 Schematic of the three-point bend test specimen used for determining the critical J-value for crack initiation. A starter crack was produced by sharpening the notch with the tip of a razor blade.

ABS particles are finely dispersed into SAN matrix (M_w = 85,000g/mol) by the emulsion process.

Single-edge notched bend (SENB) specimens are used for this study (Fig. 1). The dimensions of the injection-molded specimen are: length L = 80 mm, width W = 10 mm, and thickness B = 4 mm. The specimens are notched with a razor blade (notch tip radius = 0.2 μm). The test conditions are optimized by simulating specimen loading using a finite element method (FEM).[14,15] Based on these FEM results, the experimental parameters initial crack length a = 2 mm and support span s = 40 mm are selected. The consideration of a/W = 0.2 and s/W = 4 enables the determination of geometry-independent fracture mechanics values and minimum oscillations in load (F)-deflection (f) diagrams.

Instrumented Charpy Impact Tester

For measurements, an instrumented Charpy impact tester IKBV-4J of 4J work capacity is used, and load-deflection diagrams are recorded. The block diagram of the tester is shown in Figure 2. The weight of the hammer is 0.955 kg, the length of the hammer arm is 0.22 m, and the hammer speed at strike is 1.0 m/s. Semiconductor strain gauges are used in the striker to record the load. Deflection is followed by means of a photo-optical system. The analog load and deflection signals are amplified and then conducted to an A/D converter. Data collecting and analysis are performed using an IBM-compatible personal computer on-line, coupled to the measuring system.[16]

Flexural Mechanical Tests

Flexural tests are performed using instrumented Charpy impact tester. Five unnotched specimens

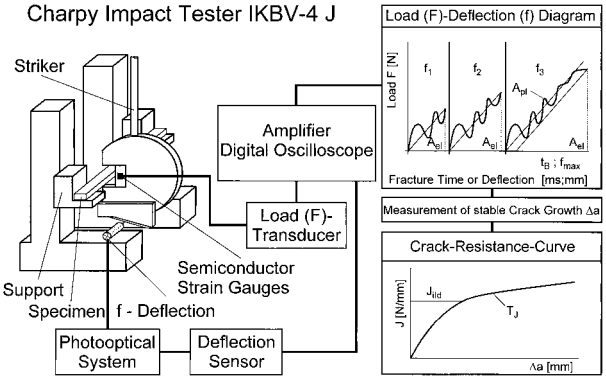

Figure 2 Fracture mechanics workplace of the computer-assisted instrumented Charpy impact test system with a stop-block arrangement.

of each composition at different temperatures are tested. The dynamic Young's modulus, E_d, and yield stress, σ_{yd}, are calculated from load–deflection curves of unnotched specimens according to the following equations:

$$E_d = \frac{F_{GY} s^3}{4BW^3 f_{GY}} \tag{1}$$

$$\sigma_{yd} = \frac{3F_{GY} s}{2BW^2} \tag{2}$$

The load F_{GY} and the deflection f_{GY} are defined by means of load–deflection diagrams at the transition point from pure elastic to elastic–plastic material behavior.

Dynamic Fracture Toughness Characterization

In elastic–plastic materials the fracture process is characterized by phases: (a) crack tip blunting; (b) crack initiation; (c) stable crack growth; and (d) unstable crack growth.

This total process can be described with the crack resistance (R) curve (Fig. 3). In principle, crack resistance curves are a function of the loading parameter (J-integral, crack opening displacement) on the stable crack growth. These curves can be determined by the loading of specimens such that stable cracks with different lengths are formed. A special experimental technique is necessary to record the dynamic crack resistance curves, which makes it possible to supply different energy values to the specimens. For this, different methods are known, but the most important is the stop block technique.[16–18] Here, different amounts of stable crack growth are produced by varying the limitation of deflection. This limitation can be accomplished by hardened steel deflection stops or by catching the pendulum hammer.

The value of J for each specimen is determined from the area under its load–deflection curve

$$J = \eta_{el}\frac{A_{el}}{B(W-a)} + \eta_{pl}\frac{A_{pl}}{B(W-a)} \times \left[1 - \frac{(0.75\eta_{el} - 1)\Delta a}{(W-a)}\right] \tag{3}$$

where

$$\eta_{el} = \frac{2F_{GY} s^2 (W-a)}{f_{GY} E_d B W^3} \Gamma^2(a/W)(1-\upsilon)^2 \tag{4}$$

and

$$\eta_{pl} = 2 - \frac{(1-a/W)(0.892 - 4.476a/W)}{1.125 + 0.892a/W - 2.238(a/W)^2} \tag{5}$$

A_{el} and A_{pl} represent the elastic and the plastic part of total deformation energy A_G. The Poisson's ratio of the whole sample, approximately given by 0.38. (a/W), depicts a fitting function correcting the finite specimen geometry.[19] Stable crack growth Δa is quantified on the fracture surface by light microscopy. The fracture surface are produced by breaking the specimens at liquid nitrogen temperature and high pendulum hammer speed.

Crack initiation, determined as the technical crack initiation at 0.2 mm crack growth by the R curve, is corresponding to J-integral values $J_{0.2}$.

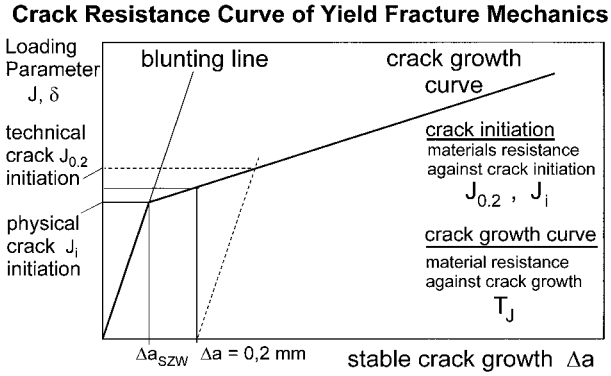

Figure 3 Crack-resistance curve of yield fracture mechanics.

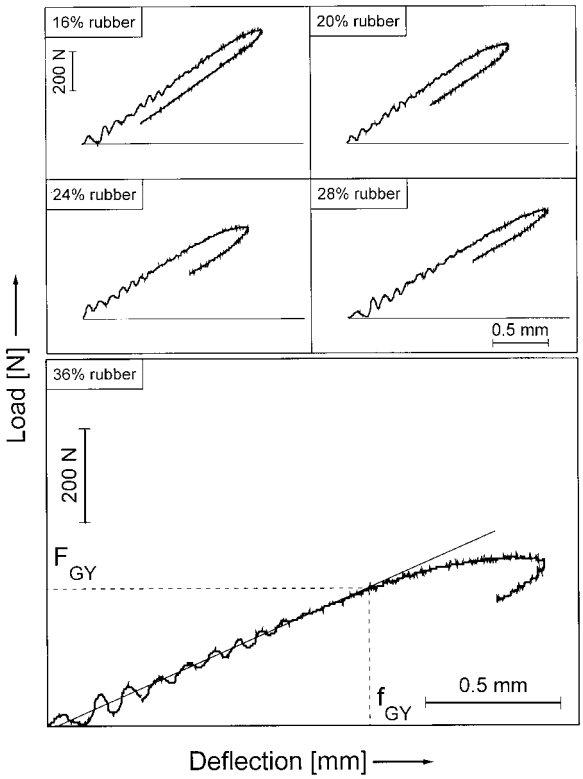

Figure 4 Load–deflection diagrams of unnotched ABS specimens with different rubber content at room temperature (F_{GY} and f_{GY}: load and deflection at transition from linear elastic to elastic-plastic behavior, respectively).

The critical crack opening displacement is determined by the Charpy impact test based on the plastic hinge model:[20]

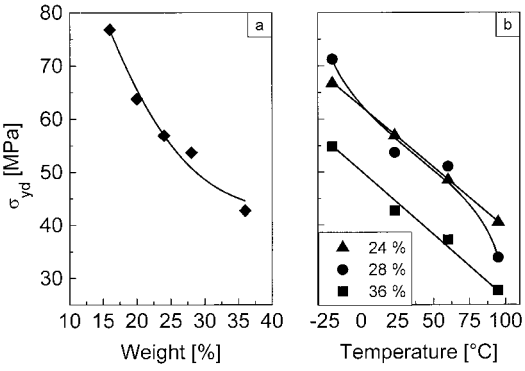

Figure 5 Dynamic yield stress, σ_{yd}, of ABS materials as a function of rubber content at room temperature (a) and as a function of temperature for rubber content of 24, 28, and 36%, respectively (b).

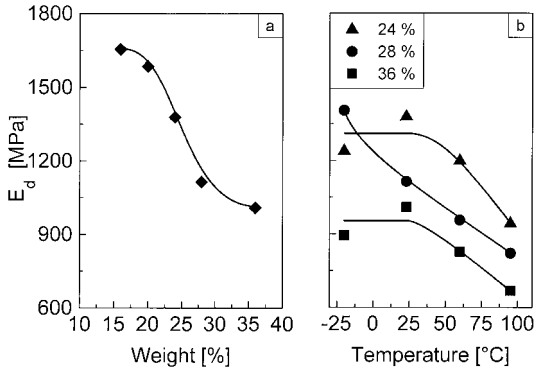

Figure 6 Dynamic Young's modulus, E_d, of ABS materials as a function of rubber content at room temperature (a) and as a function temperature for rubber content of 24, 28, and 36%, respectively (b).

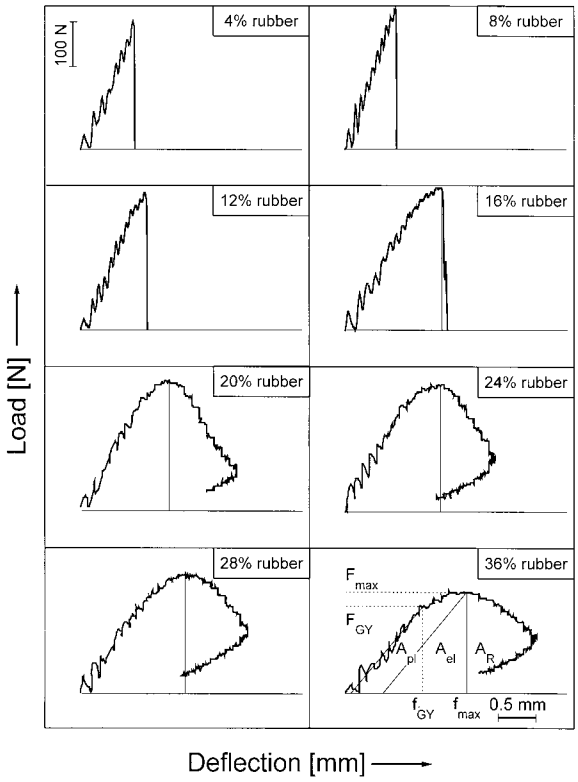

Figure 7 Load–deflection diagrams of notched ABS specimens with different rubber content at room temperature (F_{GY} and f_{GY}: load and deflection at transition from linear elastic to elastic-plastic behavior, respectively; F_{max} and f_{max}: maximum load and corresponding deflection, respectively; A_{el}, A_{pl}, and A_R: elastic and plastic part of deformation energy and crack propagation energy, respectively).

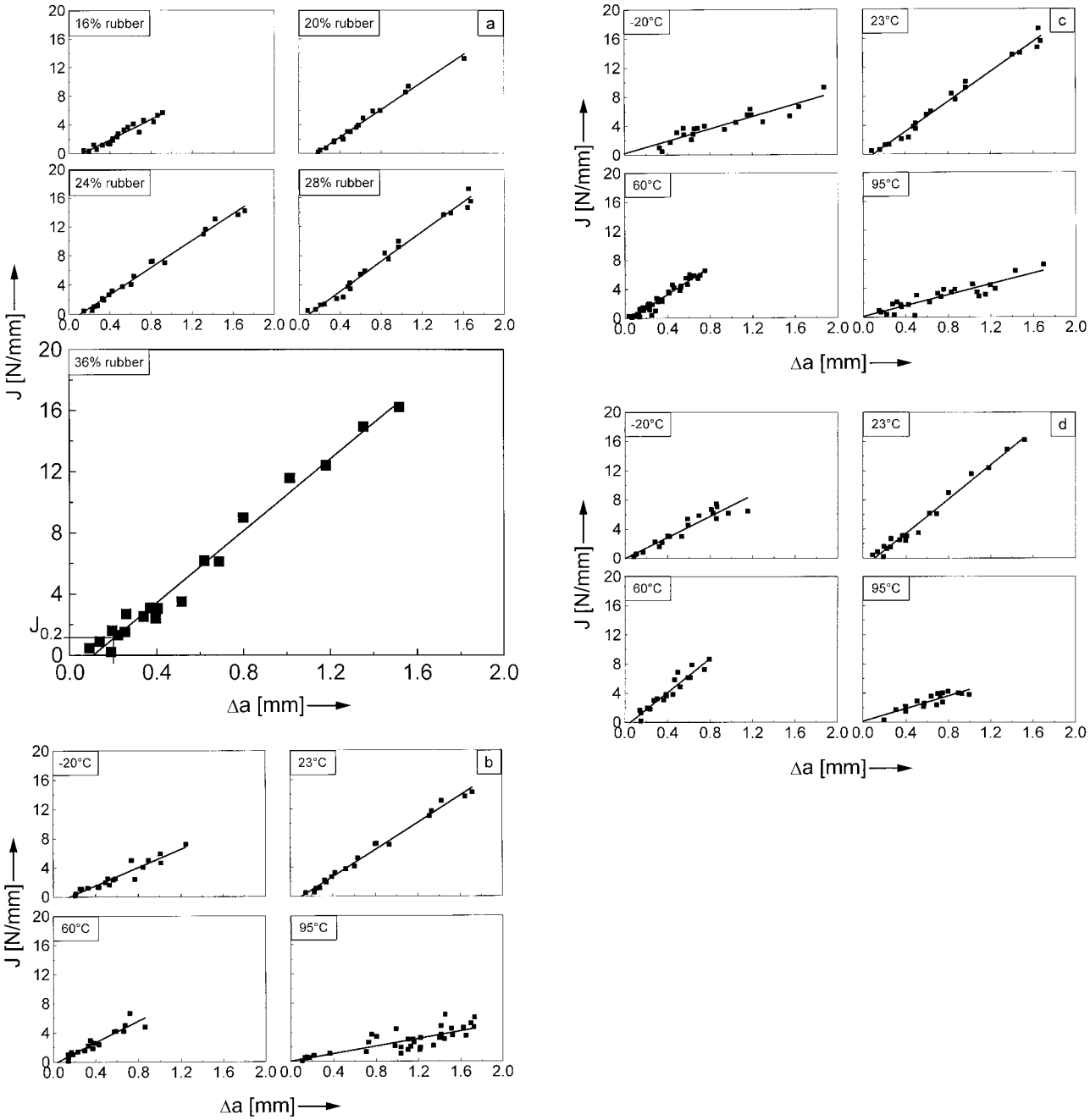

Figure 8 J–Δa curves of ABS materials of rubber content of 16, 20, 24, 28, and 36%, respectively, at room temperature (a); rubber content of 24% at different temperature (b); rubber content of 28% at different temperature (c); rubber content of 36% at different temperature. (d) ($J_{0.2}$: J-integral value as resistance against stable crack initiation determined at engineering crack initiation point of $\Delta a = 0.2$ mm).

$$\delta = \frac{1}{n}(W - a)\frac{4f_{\max}}{s} \tag{6}$$

where n is the rotational factor ($n = 4$).

For polymeric materials with large plastic deformation, only processes in the crack tip should be considered in calculating the critical crack opening displacement. This is due to the fact that differences between the actual crack opening displacement and that calculated from maximum deflection, $f_{\max}$, will increase with increasing plastic deformation. This critical value is denoted

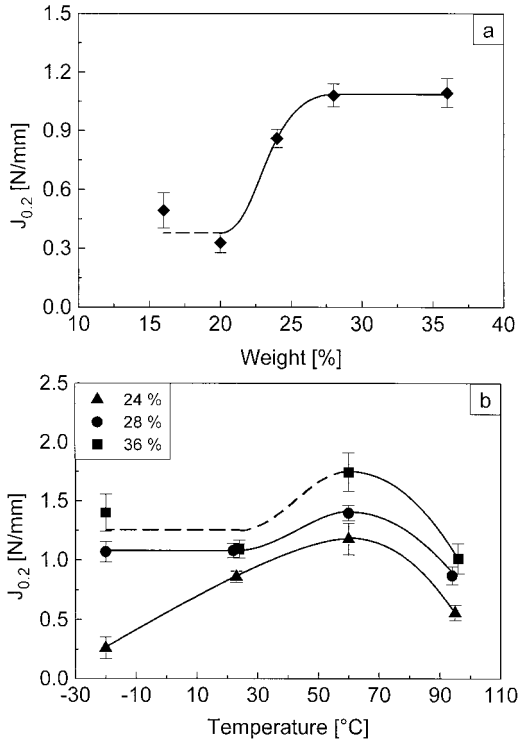

Figure 9 The critical J-integral initiation value, $J_{0.2}$, as a function of rubber content at room temperature (a) and as a function of temperature for rubber content of 24, 28, and 36%, respectively (b).

as δ_{dk}. To determine δ_{dk}, it is necessary to substitute the maximum deflection, $f_{\max}$, by the notch contribution of deflection, f_k.[21] The notch contribution, f_k, is calculated by:

$$f_k = f_{\max} - f_b \tag{7}$$

where f_b is the deflection of the unnotched specimen:

$$f_b = \frac{F_{\max} s^3}{4BW^3 E_d} \tag{8}$$

The crack initiation value, $\delta_{0.2}$, is the value of at crack growth of 0.2 mm.

RESULTS AND DISCUSSION

Mechanical Properties

Figure 4 shows the load–deflection diagrams of unnotched specimens with a rubber content of 16, 20, 24, 28, and 36%, respectively, at room temperature. For each composition, all the specimens are not broken under the test conditions. From these curves, one can see that the maximum load decreases with increasing the rubber content as well as the maximum deflection increases with increasing the rubber content. This reflects that the material becomes more elastic–plastic with increasing the rubber content.

The dynamic Young's modulus, E_d, and yield stress, σ_{yd}, are calculated from load–deflection curves at the transition point from pure elastic to elastic–plastic material behavior according to eqs. (1) and (2), respectively. Figure 5(a) and (b) illustrate the variation of σ_{yd} with the rubber content and temperature, respectively. σ_{yd} decrease both with increasing rubber content and temperature. The variation of E_d with rubber content and temperature is demonstrated in Figure 6(a) and (b), respectively. E_d tends to decrease with increasing rubber content and temperature.[22]

Load–Deflection Diagrams of Notched Specimens

Figure 7 shows load–deflection diagrams of room temperature for ABS materials with particle diameter of 330 nm and rubber content of 4, 8, 12, 16, 20, 24, 28, and 36%, respectively. It can be seen from Figure 7 that all those with rubber content of 4 and 8% possess a linear load–deflection curve up to a maximum, followed by an unstable crack propagation, which is indicated by a nearly vertical drop in the load–deflection curve. It is expected that fractures are brittle in nature. The main deformation process is elastic deformation, and the dominant crack growth mechanism is unstable crack propagation. For those with a rubber content of 12 and 16%, even though the materials break in a brittle fashion and the crack growth mechanism is still unstable crack propagation, the materials deformation behavior is elastic–plastic. For those with a rubber content higher than 20%, the materials do not break under the test condition, and the deformation behavior is elastic–plastic. The crack growth mechanism is stable crack propagation. Therefore, the diagram shows two transitions of mechanical behavior. The first transition occurs from pure elastic (SAN with 4 and 8% rubber) to elastic–plastic material behavior with predominantly unstable crack growth (SAN with 12 and 16% rubber). In these regions the specimens break in a brittle manner. The second transition to predominantly stable crack growth without sample fracture is characterized by means of the large crack propa-

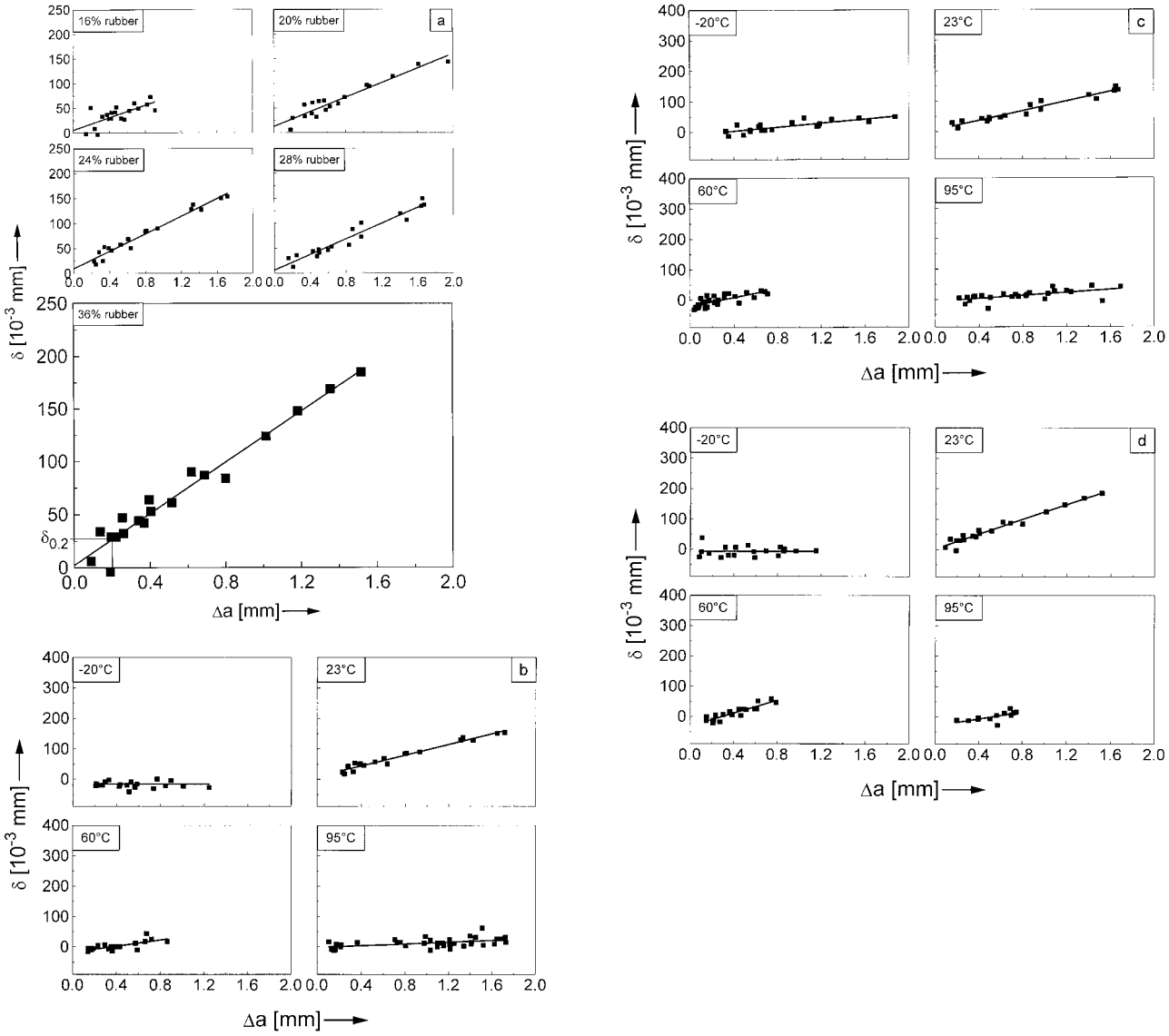

Figure 10 δ–Δ*a* curves of ABS materials of rubber content of 16, 20, 24, 28, and 36%, respectively, at room temperature (a); rubber content of 24% at different temperature (b); rubber content of 28% at different temperature (c); rubber content of 36% at different temperature (d) ($\delta_{0.2}$: COD value as resistance against stable crack initiation determined at engineering crack initiation point of $\Delta a = 0.2$ mm).

gation energies, A_R (SAN with 20, 24, 28, and 36% rubber). The decreasing deflection values at the end of the experiment are caused by reflection of the pendulum striker from the sample. Therefore, the second transition can be designated brittle-to-tough transition.

From this load–deflection behavior it may be deduced that a uniform toughness characterization of these materials depending on concentration is not possible, if one considers previous knowledge of the use of different fracture mechanical concepts. The toughness characterization of those with lower rubber content must be carried out with fracture mechanics values that characterize materials resistance, as proposed to unstable crack growth, because of the dominant unstable crack growth mechanism (for instance, *J*-integral, the evaluation method of Sumpter and Turner[23]). The toughness characterization of those with higher rubber content must be accomplished using crack resistance (*R*) curves.

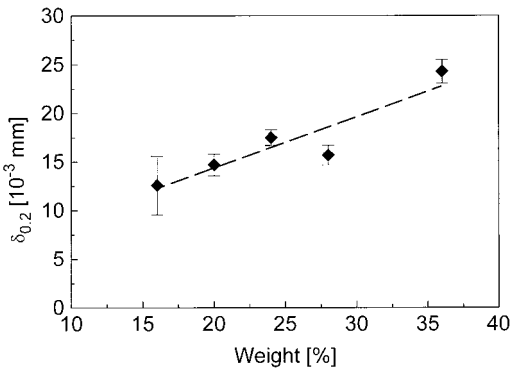

Figure 11 The critical initiation value, $\delta_{0.2}$, as a function of rubber content at room temperature.

Fracture Toughness

Figure 8(a) shows the J–Δa curves of ABS materials with rubber content of 16, 20, 24, 28, and 36%. Figure 8(b), (c), and (d) illustrate the J–Δa curves for rubber content of 24, 28, and 36% at different temperatures, respectively. From these curves, one can see that there is a good linear relationship between J and Δa. The critical J-integral value, $J_{0.2}$, is determined at $a = 0.2$ mm.

The variation of the $J_{0.2}$ values with the rubber content is shown in Figure 9(a) at room temperature. The $J_{0.2}$ value tends to increase with increasing ABS content. This implies that the rubber particles in ABS provide toughening effect for the brittle matrix.

The effect of temperature on $J_{0.2}$ is shown in Figure 9(b). $J_{0.2}$ values of all rubber contents first increase with increasing temperature; after reaching the maximum values at the temperature of 60°C, all decrease with further increasing temperature. The decrease of $J_{0.2}$ value at high temperature is caused by, on the one hand, reduction of the Young's modulus, and on the other hand, the embrittlement of the SAN matrix at temperatures near its glass transition.[24]

Crack Opening Displacement (COD)

Figure 10(a) illustrates the δ–Δa curves of ABS materials with a rubber content of 16, 20, 24, 28, and 36%. Figure 10(a), (b), and (c) are δ–Δa curves for a rubber content of 24, 28, and 36% ABS materials at different temperatures, respectively. A good linear relationship between δ and Δa can be observed from these curves. The critical δ value, $\delta_{0.2}$, is determined at $\Delta a = 0.2$ mm.

The variation of the $\delta_{0.2}$ values with the rubber content is shown in Figure 11. The $\delta_{0.2}$ value tends to increase with increasing ABS content.

$\delta_{0.2}$ values reach the maximum value at room temperature. At all other temperatures, all $\delta_{0.2}$ values are nearly zero.

From above results, one can see that rubber toughening is one of the most successful methods of modifying the properties of brittle polymers. Toughening mechanisms include crazing and shear yielding, both of which involve localized deformation of brittle matrix associated with stress concentrations initiated by the rubber inclusions. Dispersed rubber particles toughen the matrix mainly by inducing an extensive combined crazing and yielding in SAN. It has been reported in the literature that shear yielding in the polymer matrix absorbs a large amount of the impact energy, thereby enhancing the toughness of the thermoplastic/rubber blends.[25,26]

Fractography

The following features of the fracture surface can be observed under SEM: razor-sharpened notch, stretch zone, crack growth, stress whitening zone, and undamaged zone. Figure 12 is a schematic diagram showing formation of various zones in the fracture surface.

During initial loading of a fracture mechanics specimen, crack tip blunting causes the formation of a stretched zone at the crack tip prior to actual crack initiation/propagation. Several authors have proposed measurement of the stretch zone width (SZW) to determine the characteristic frac-

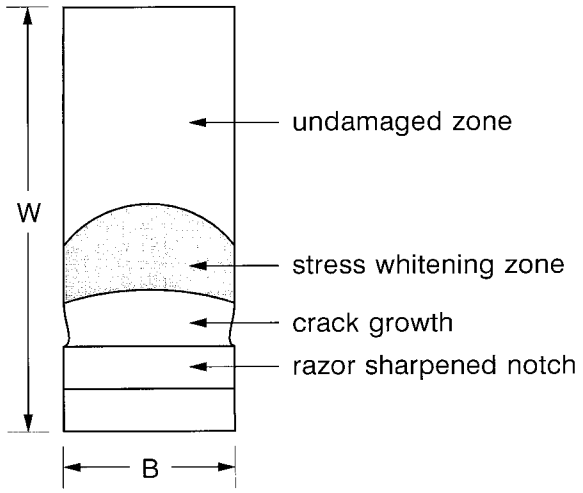

Figure 12 Schematic diagrams showing formation of various zones ahead of the crack tip (B and W: specimen thickness and width, respectively).

ture mechanics value corresponding to physical crack initiation. The stretch zone width increases with the loading, and will extend to the critical with (SZW_c) value, which is achieved at the crack initiation point. Figure 13 shows the process of stretch zone formation.

When the applied load above a certain level, a stress whitening zone occurs ahead of the initial crack tip. This crack tip stress whitening zone continues to exist and to grow even after crack initiation. The sketch of the fracture surface shows that the boundary line between the crack growth and the crack tip stress whitening zone is well defined, and the crack growth front advances evenly across the whole specimen.

It is well-known that ductile fracture, starting from a preexisting crack, may be preceded by the following four phases: (1) blunting of the crack and forming a stretch zone, followed by (2) initiation of crack growth, which then evolutes into (3) stable crack propagation, and the stable crack propagation continues by shift of the whole crack front, finally ends with (4) unstable and rapid crack propagation (Fig. 14).

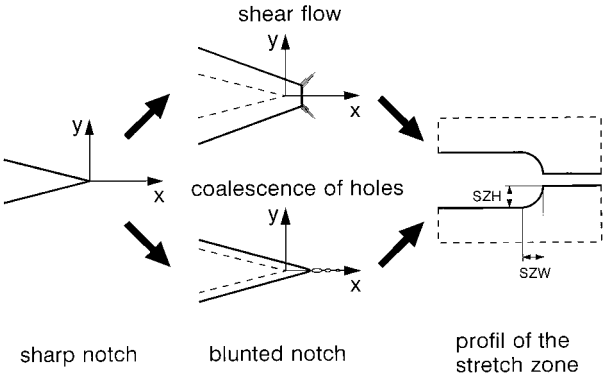

Figure 13 Schematic process of stretch-zone formation.

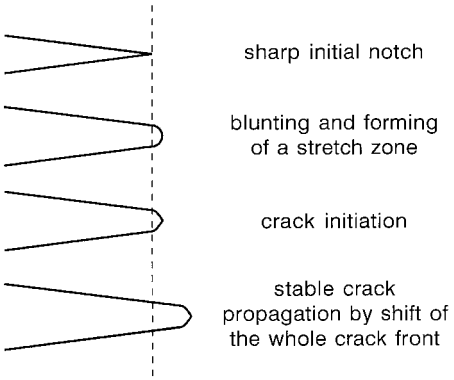

Figure 14 Crack initiation and propagation process.

CONCLUSIONS

The effect of rubber content and temperature on dynamic fracture toughness of ABS materials has been investigated by the use of instrumented impact Charpy tester. It is shown that the materials exhibited a different toughness behavior, depending on rubber content and temperature. The resistance against stable crack initiation ($J_{0.2}$ or $\delta_{0.2}$) increases with increasing rubber content. However, $J_{0.2}$ first increases with increasing temperature, after reaching the maximum value, it decreases with increasing temperature again. The decrease of $J_{0.2}$ value at high temperature is caused by, on the one hand, reduction of the Young's modulus, and on the other hand, the embrittlement of the SAN matrix at temperatures near its glass transition.

The Bayer AG, Leverkusen, more especially Dr. P. Krüger, is gratefully acknowledged for making available the ABS materials. Dr. Y. C. Han wishes to thank the DAAD-K. C. Wong Foundation for her research fellowship at Martin-Luther-University Halle-Wittenberg.The authors also acknowledge financial support from Deutsche Forschungsgemeinschaft (DFG).

REFERENCES

1. Bucknall, C. B. Toughened Plastics; Applied Science Publishers: London, 1977.
2. Rice, J. R. J Appl Mech 1968, 35, 379.
3. Begley, J. A.; Landes, J. D. ASTM STP 1972, 514, 1.
4. Hodgkinson, J. M.; Williams, J. G. J Mater Sci 1980, 16, 50.
5. Hashemi, S.; Williams, J. G. Polym Eng Sci 1986, 26, 760.
6. Narisawa, I. Polym Eng Sci 1987, 27, 41.
7. Huang, D. D.; Williams, J. G. Polym Eng Sci 1990, 30, 1341.
8. Lee, C. B.; Chang, F. C. Polym Eng Sci 1992, 32, 792.
9. ASTM Standard E813–81. Annual Book ASTM Standards 1981, Part 10, 822.
10. ASTM Standard E813–87. Annual Book ASTM Standards 1987, Part 10, 968.
11. ASTM Standard E813–89. Annual Book ASTM Standards 1989, Part 10, 628.
12. Lee, C. B.; Lu, M. L.; Chang, F. C. J Appl Polym Sci 1993, 47, 1867.
13. Lu, M. L.; Lee, C. B.; Chang, F. C. Polym Eng Sci 1991, 43, 1111.

14. Grellmann, W.; Sommer, J. P. Chemnitz 1985, 17, 48.
15. Grellmann, W.; Sommer, J.-P.; Hoffmann, H.; Michel, B. In Proceedings 1st Conference on Mechanics, Prague, June 29–July 3, 1987, p. 129, vol. 5.
16. Grellmann, W.; Seidler, S. Mater Prufung/Mater Testing 1991, 33, 213.
17. Savadori, A.; Bramuzzo, M.; Marega, C. Polym Testing 1984, 4, 73.
18. Seidler, S.; Grellmann, W. Polym Testing 1995, 14, 453.
19. Blumenauer, H.; Pusch, G. Technische Bruchmechanik; Deutscher Verlag für Grundstoffindustrie: Leipzig, 1993.
20. Kobayashi, T. Eng Fracture Mech 1984, 16, 67.
21. Grellmann, W.; Jungbluth, M. Chemnitz 1987, 37, 186.
22. Han, Y.; Lach, R.; Grellmann, W. Angew Makromol Chemie/Appl Macromol Chem Phys, to appear.
23. Sumpter, J. D. G.; Turner, C. E. ASTM STP 1976, 601, 3.
24. Michler, G. H. Kunststoff-Mikromechanik. Morphologie, Deformations- und Bruchverhalten; Carl Hanser Verlag: München, 1992, p. 172.
25. Parker, D. S.; Sue, H. J.; Huang, H.; Yee, A. F. Polymer 1990, 31, 2267.
26. Sue, H. J.; Yee, A. F. J Mater Sci 1991, 26, 3449.